Available online at www.sciencedirect.com

SciVerse ScienceDirect

Ceramics International 38 (2012) 6487–6494

CERAMICS INTERNATIONAL

www.elsevier.com/locate/ceramint

Synthesis, structural analysis and dielectric properties of $Ba_8(Mg_{1-x}Zn_x)Nb_6O_{24}$ hexagonal perovskites

Sam Solomon[a,b,*], M.K. Suresh[a,c], J.K. Thomas[a], V.S. Prasad[d], P.R.S. Wariar[c]

[a]Department of Physics, Mar Ivanios College, Thiruvananthapuram, Kerala 695015, India
[b]Department of Physics, St. John's College, Anchal, Kerala 691306, India
[c]Department of Physics, University College, Thiruvananthapuram, Kerala 695034, India
[d]Chemical Sciences & Technology Division, National Institute for Interdisciplinary Science & Technology, Thiruvananthapuram, Kerala 695019, India

Received 25 July 2011; received in revised form 4 April 2012; accepted 8 May 2012
Available online 17 May 2012

Abstract

$Ba_8(Mg_{1-x}Zn_x)Nb_6O_{24}$ ($x=0$, 0.2, 0.4, 0.6, 0.8 and 1) ceramics were prepared through the conventional solid-state route. The materials were calcined at 1250 °C and sintered at 1375–1425 °C. The structure of the system was analyzed using X-ray diffraction and vibrational spectroscopic studies. The microstructure of the sintered pellet was analyzed using scanning electron microscopy. The dielectric constant (ε_r), temperature coefficient of resonant frequency (τ_f) and the unloaded quality factor (Q_u) were measured in the microwave frequency region. The τ_f values of the compositions were reduced by varying the value of x from 0 to 1. The dielectric responses to frequency were also studied in the radio frequency region. The compositions have good microwave dielectric properties and hence are suitable for dielectric resonator applications.

Keywords: A. Sintering; B. Spectroscopy; C. Dielectric properties; D. Perovskites

1. Introduction

Because of the rapid development in mobile communication and satellite broadcasting systems, the design of high-quality devices is very important. In order to achieve miniaturization of the dimensions of the devices and for high efficiency and stability, much research has focused on developing dielectric materials with a high quality factor ($Q_u \times f$), a high dielectric constant (ε_r) and a low temperature coefficient of resonant frequency (τ_f) for dielectric resonators (DR) and microwave substrates [1–6]. The compounds with complex perovskite type structure are widely used in the area of wireless communication systems. The materials such as $Ba(Mg_{1/3}Ta_{2/3})O_3$, $Ba(Zn_{1/3}Ta_{2/3})O_3$ and $Ba(Zn_{1/3}Nb_{2/3})O_3$ are the examples of these kinds of compounds [7–12]. Extensive work has been going on the tantalum and niobium based cubic perovskite ceramics because of their high polarizability produced by multiple bonding to oxygen and wide compositional tuning opportunities offered by the substitutional flexibility of mixed B-site perovskites.

Several investigators have reported that the processing of $Ba(Zn_{1/3}Ta_{2/3})O_3$-based systems at high temperature is accompanied by the formation of secondary phases such as $Ba_8ZnTa_6O_{24}$, $BaTa_2O_6$, $Ba_5Ta_4O_{15}$, $Ba_3Ta_2O_8$, etc. by the volatilization of ZnO [13–17]. Similarly, Hughes et al. [18] reported that two major secondary phases, $Ba_5Nb_4O_{15}$ and $Ba_8ZnNb_6O_{24}$, were found on the surface of sintered $Ba(Zn_{1/3}Nb_{2/3})O_3$–$Ba(Ga_{1/2}Ta_{1/2})O_3$ ceramics as a result of Zn evaporation and the phase $Ba_8ZnNb_6O_{24}$ is consistent with the findings of Davies et al. [19] and Bieringer et al. [20] for the $Ba(Zn_{1/3}Ta_{2/3})O_3$ analogue system. They reported that $Ba_8ZnNb_6O_{24}$ exhibits hexagonal structure with space group $P6_3cm$ and lattice parameters $a=10.0643$ Å and $c=19.0060$ Å. Barwick et al. [21] reported that $Ba(Ni_{1/3}Nb_{2/3})O_3$–$Ba(Zn_{1/3}Nb_{2/3})O_3$ shows a secondary phase $Ba_8ZnNb_6O_{24}$, which is formed to compensate for

*Corresponding author at: Mar Ivanios College, Department of Physics, Thiruvananthapuram, Anchal, Kerala 695015, India.
Tel.: +91 9847314237; fax: +91 471 2532445.
E-mail address: samdmrl@yahoo.com (S. Solomon).

0272-8842/$36.00 © 2012 Elsevier Ltd and Techna Group S.r.l. All rights reserved.
http://dx.doi.org/10.1016/j.ceramint.2012.05.026

the Zn vacancies resulting from the lost material during processing. This is analogous to $Ba_8ZnTa_6O_{24}$, the impurity phase found in $Ba(Zn_{1/3}Ta_{2/3})O_3$ ceramics during high temperature processing. The $Ba_8ZnNb_6O_{24}$ is a perovskite-type structure, with regular stacking faults, giving recurrent planes of face-sharing (as opposed to corner-sharing) oxygen octahedra. Kawaguchi et al. [22] studied the microwave dielectric properties of $Ba_8Ta_6(Ni_{1-x}M_x)O_{24}$ (M=Zn and Mg; x=0–1) solid solutions and they could reduce the τ_f value towards 18 ppm/°C for the value Mg=1. Recently Suresh et al. [23] studied the structural and dielectric properties of $Ba_8Zn(Nb_{6-x}Sb_x)O_{24}$ ceramics and the τ_f value is reduced to −3.6 ppm/°C for x=2.4. By the Sb substitution for Nb in $Ba_8MgNb_6O_{24}$, the τ_f value could be reduced from +66.1 to +1.5 ppm/°C [24]. In the present paper, we report the synthesis, characterization and dielectric properties of $Ba_8(Mg_{1-x}Zn_x)Nb_6O_{24}$ (x=0, 0.2, 0.4, 0.6, 0.8 and 1) ceramics.

2. Experimental

$Ba_8(Mg_{1-x}Zn_x)Nb_6O_{24}$ (x=0, 0.2, 0.4, 0.6, 0.8 and 1) ceramics are prepared through the conventional solid-state ceramic route. The high purity (>99%) $BaCO_3$, MgO, ZnO and Nb_2O_5 are weighed in stoichiometric ratios and ball milled, using zirconia balls in plastic containers and acetone as wetting medium, for 2 h. The samples are dried and calcined at 1250 °C for 6 h in electrically heated furnace. The calcined powder is again ball milled for 6 h and the slurry is dried and ground well in agate mortar. Polyvinyl alcohol (5 wt%) is added to this powder as a binder, again ground well and dried. The powder is then pressed in the form of cylindrical pellets at a pressure of 100 MPa using hydraulic press. The pellets are then sintered at the temperature 1375–1425 °C for 4 h in a controlled heating schedule of 4 °C/min up to 600 °C, soaking for half-an hour to expel the binder and then to the sintering temperature at a heating rate of 5 °C/min. The samples are then cooled to room temperature. The sintered samples are polished well and the densities are calculated by the Archimedes method. Powdered samples are used for X-ray diffraction (XRD) studies using CuKα radiation (Philips Expert Pro). The lattice parameters are calculated from XRD data using least square method. The infrared (IR) spectra of the samples are recorded in the range 400–2000 cm^{-1} on a Perkin Elmer Fourier Transform Infrared (FT-IR) Spectrometer (Spectrum RX1) using KBr pellet method. Polished samples are thermally etched at a temperature 50 °C below the sintering temperature and used for Scanning Electron Microscope (SEM) and Energy Dispersive Spectrum (EDS) (JEOL Model 6390 LV) studies. Sintered and polished samples were used for microwave dielectric property measurements using an Agilent Network Analyzer (Agilent Technologies, Model no. 8753ET Inc., Palo Alto, CA). The test ceramics are discs of ~12 mm diameter and ~6 mm thickness with aspect ratio (D/L) of ~2. The specimen was placed on a quartz cylinder fixed at the centre of a cylindrical invar cavity whose size is 3–4 times greater than it. The dielectric constant (ε_r) was measured by the post resonator method of Hakki and Coleman [25] using the $TE_{01\delta}$ mode of

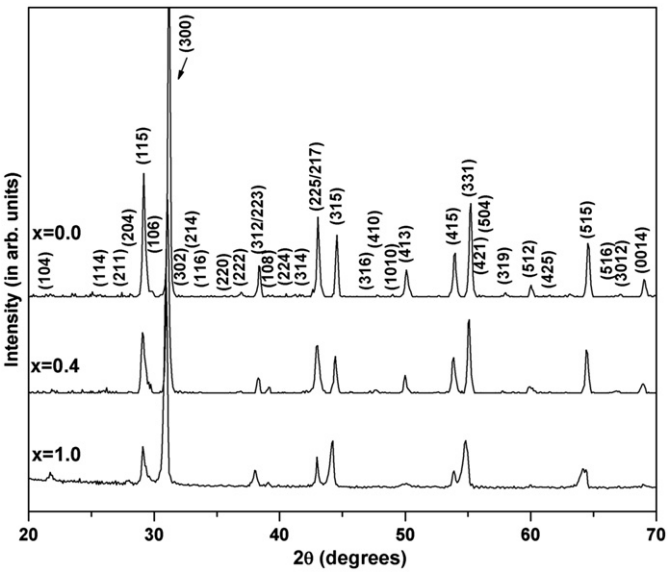

Fig. 1. XRD patterns of $Ba_8(Mg_{1-x}Zn_x)Nb_6O_{24}$ ceramics.

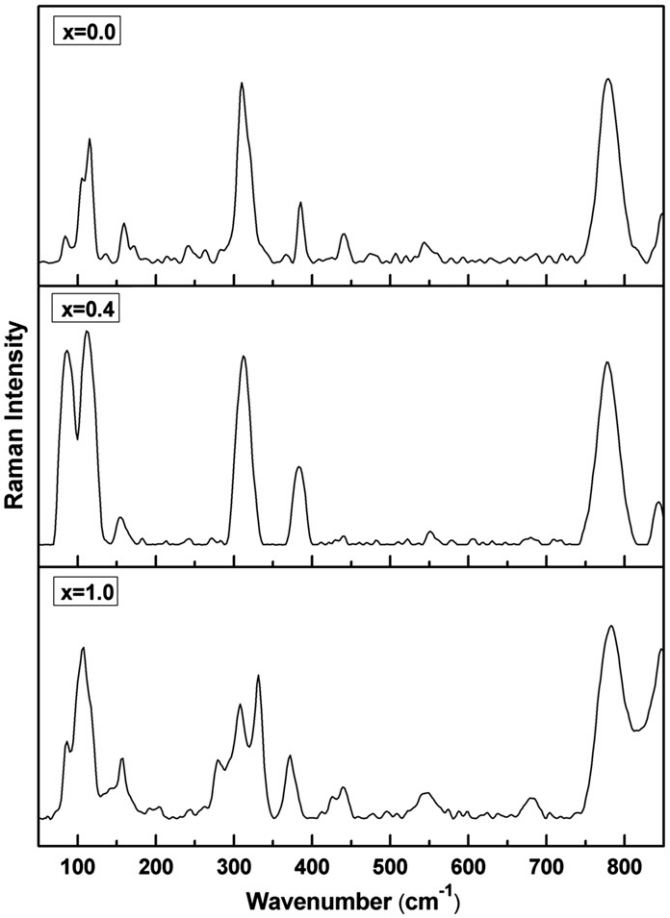

Fig. 2. Raman spectra of $Ba_8(Mg_{1-x}Zn_x)Nb_6O_{24}$ ceramics.

resonance coupled through E-field probes as described by Courtney [26]. The unloaded quality factor (Q_u) of resonance was determined using a resonance cavity method proposed by Krupka et al. [27]. The measurements were made in the frequency range 4–6 GHz. In the end-shorted position, the sample is heated from room temperature to 80 °C, and the resonant frequency is noted at every 5 °C interval and the temperature coefficient of resonant frequency is calculated. The radio frequency dielectric properties of the samples are studied using an LCR meter (Hioki-3532–50) in the frequency range 50 Hz–5 MHz. For the studies, pellets of diameter ~12 mm and thickness < 2 mm are made in the form of a disc capacitor with the specimen as the dielectric medium with silver electrodes on both sides of the circular disc.

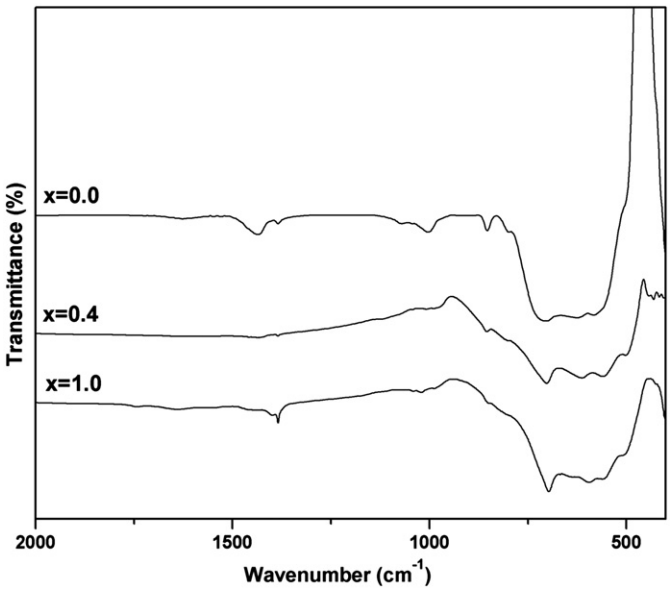

Fig. 3. FT-IR spectra of $Ba_8(Mg_{1-x}Zn_x)Nb_6O_{24}$ ceramics.

3. Results and discussion

The XRD patterns of sintered $Ba_8(Mg_{1-x}Zn_x)Nb_6O_{24}$ ($x=0$, 0.4 and 1) ceramics are given in Fig. 1. All the peaks can be indexed using the structure of $Ba_8Ta_6NiO_{24}$ ceramics (ICDD file no. 89-0693), a hexagonal perovskite structural (space group $P63cm$) material based on an 8H $(cchc)_2$ close packed arrangement of BaO_3 layers, with $Z=3$ [19,28,29]. Kawaguchi et al. [22] reported that $Ba_8Ta_6(Ni_{1-x}Zn_x)O_{24}$ solid solutions did not show any secondary phase in the composition range $x=0$–1, but $Ba_8Ta_6(Ni_{1-x}Mg_x)O_{24}$ showed several secondary phases in the same range. Moreover, they reported that there is peak shift towards the lower 2θ values with Zn and Mg substitutions for Ni. In the present system, it is clear from Fig. 1 that there is no peak shift and structural change with the increasing value of x and no additional phases are present in the composition range $x=0$–1. The crystallographic parameters and densities of $Ba_8MgNb_6O_{24}$ ($x=0$) and $Ba_8ZnNb_6O_{24}$ ($x=1$) are given in our previous reports [23,24]. In $Ba_8(Mg_{0.6}Zn_{0.4})Nb_6O_{24}$ ($x=0.4$), the lattice parameters are calculated as $a=9.9959$ Å and $c=19.4617$ Å.

The Raman spectra of $Ba_8(Mg_{1-x}Zn_x)Nb_6O_{24}$, $x=0.0$, 0.4 and 1.0, are recorded over the range 50–900 cm^{-1} and

Table 1
Raman spectral data of $Ba_8MgNb_6O_{24}$, $Ba_8(Mg_{0.6}Zn_{0.4})Nb_6O_{24}$ and. $Ba_8ZnNb_6O_{24}$ and their assignments.

Wavenumber (cm^{-1})			Band assignments
$Ba_8MgNb_6O_{24}$	$Ba_8(Mg_{0.6}Zn_{0.4})Nb_6O_{24}$	$Ba_8ZnNb_6O_{24}$	
848 m	845 m	849 s	$\nu_1 A_{1g}$
779 vs	780 vs	785 vs	
686 vw	680 w	681 w	$\nu_3 F_{1u}$
543 wbr	551 wbr	549 wbr	$\nu_2 E_g$
474 vw			$\nu_4 F_{1u}$
440 m	441 vw	442 w	
		425 w	
		411 vw	
385 m	385 m	375 m	$\nu_5 F_{2g}$
		333 s	
310 vs	314 vs	310 s	
263 vw	271 vw	281 m	$\nu_6 F_{2u}$
242 w	243 vw	244 vw	
		203 vw	
160 m	155 w	159 m	Lattice mode
115 s	114 vs		
105 m		109 vs	
85 w	88 s	86 m	

shown in Fig. 2. The IR spectra of the above three compositions over the range 400–4000 cm^{-1} are shown in Fig. 3. The observed spectral data in the Raman and IR spectra and their assignments are given in Tables 1 and 2, respectively. All the three samples show almost similar Raman and IR spectra. This observation is in good agreement with the XRD measurements where all the samples have the same hexagonal perovskite structure. Earlier report [29] shows that these types of compounds have two different pairs of face sharing octahedra. In the first pair, one octahedron is occupied by Nb atoms and the other one is empty. In the second pair, one of the octahedra is occupied by Nb atoms while the other is occupied by Mg atoms for the $x=0.0$ compound, Zn atoms for the $x=1.0$ compound and Mg/Zn for $x=0.4$ compound, or Nb or a vacancy. This leads to the presence of distorted as well as undistorted close to ideal octahedra in the compounds. As a consequence, splitting of degenerate and non-degenerate levels and activation of inactive modes can be expected in the Raman and IR spectra of the compounds.

The six fundamental vibrations of the octahedron with O_h symmetry are distributed as [30,31], $\Gamma = A_{1g}(R)+E_g(R)+2F_{1u}(IR)+F_{2g}(R)+F_{2u}$(silent). The Raan active v_1A_{1g}, v_2E_g, and v_5F_{2g} modes of vibration of the octahedra are observed as intense bands in the Raman spectra of all the three compounds. The symmetric stretching mode of vibration v_1A_{1g} is observed as a doublet with components around 846 and 782 cm^{-1}. The v_2E_g mode due to the antisymmetric stretching vibration of the octahedra is weak, broad and centered at 543, 551 and 549 cm^{-1} in the $x=0.0$, 0.4 and 1.0 compounds, respectively. The symmetric bending v_5F_{2g} mode is observed with triplet or doublet structure in the range 310–385 cm^{-1}. The bands in this region are strong and medium in intensity. The v_1A_{1g} and v_2E_g modes have become active in the IR spectrum and are observed as less intense bands in the corresponding region.

In the IR spectra, strong absorption bands with doublet structure are observed in all the compounds in the range 612–704 cm^{-1} due to the antisymmetric stretching vibration of the octahedra, the v_3F_{1u} mode. The IR active v_4F_{1u} mode of vibration due to the antisymmetric bending of the octahedron is observed as shoulders at 503 and 506 cm^{-1} in the $x=0.0$ and $x=1.0$ compounds and as a doublet in the $x=0.4$ compound with components at 502 and 431 cm^{-1}. The silent mode v_6F_{2u} has become active in the Raman spectrum and is observed as very weak band with triplet or doublet structure around 242 cm^{-1}. The lattice modes are observed below 160 cm^{-1}.

The effect of Zn substitution for Mg on the microwave dielectric properties of $Ba_8(Mg_{1-x}Zn_x)Nb_6O_{24}$ ceramics is shown in Fig. 4 and the details are given in Table 3. As the x value increases from 0 to 1, the $Q_u \times f$ values decrease from 18000 to 10890 GHz. The τ_f values of the samples decreased from 66.1 to 49.9 ppm/°C depending on the composition x; any significant variations in the dielectric constant were not observed with the Zn substitution for Mg. The experimental density of each sample is given in Table 3 and which is greater than 95% of the theoretical values.

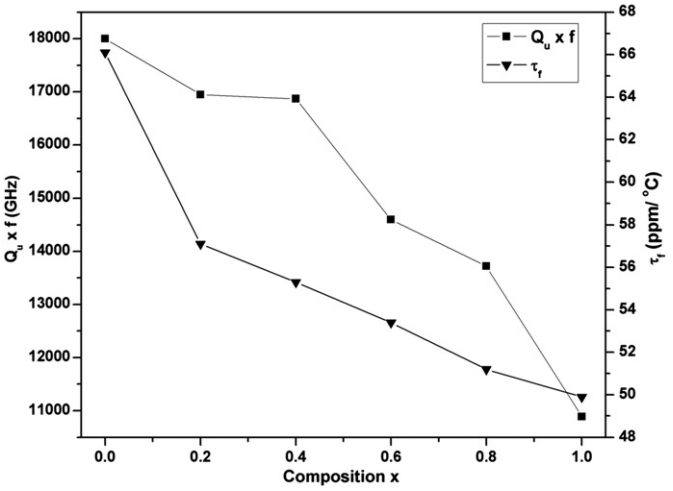

Fig. 4. Effect of Zn substitution for Mg on quality factor ($Q_u \times f$) and temperature coefficient of resonant frequency (τ_f).

Table 2
IR spectral data of $Ba_8MgNb_6O_{24}$, $Ba_8(Mg_{0.6}Zn_{0.4})Nb_6O_{24}$ and $Ba_8ZnNb_6O_{24}$ and their assignments.

Wavenumber (cm^{-1})			Band assignments
$Ba_8MgNb_6O_{24}$	$Ba_8(Mg_{0.6}Zn_{0.4})Nb_6O_{24}$	$Ba_8ZnNb_6O_{24}$	
853 w 798 w	854 w 799 sh	850 w	v_1A_{1g}
704 s 625 s	703 s 612 s	697 s 641 m	v_3F_{1u}
583 s			v_2E_g
	559 s	596 s 556 s	
503 sh	502 m 431 w	506 brsh	v_4F_{1u}

Table 3
Microwave dielectric properties of $Ba_8(Mg_{1-x}Zn_x)Nb_6O_{24}$ (x=0, 0.2, 0.4, 0.6, 0.8 and 1) ceramics.

x	Dimensions		Experimental density (g/cm^3)	Resonant frequency f (GHz)	$Q_u \times f$ (GHz)	Dielectric constant (ε_r)	τ_f (ppm/°C)
	Thickness $\times 10^{-3}$ (m)	Diameter $\times 10^{-3}$ (m)					
0	6.34	12.45	6.0689	4.04	18000	35.91	+66.1
0.2	6.10	12.40	6.1201	4.08	16950	36.05	+57.1
0.4	6.65	12.41	6.1367	3.95	16870	37.07	+55.3
0.6	6.21	12.43	6.1861	4.00	14600	37.01	+53.4
0.8	7.10	12.53	6.2003	3.86	13720	37.03	+51.2
1	6.60	12.58	6.0783	3.96	10890	36.26	+49.9

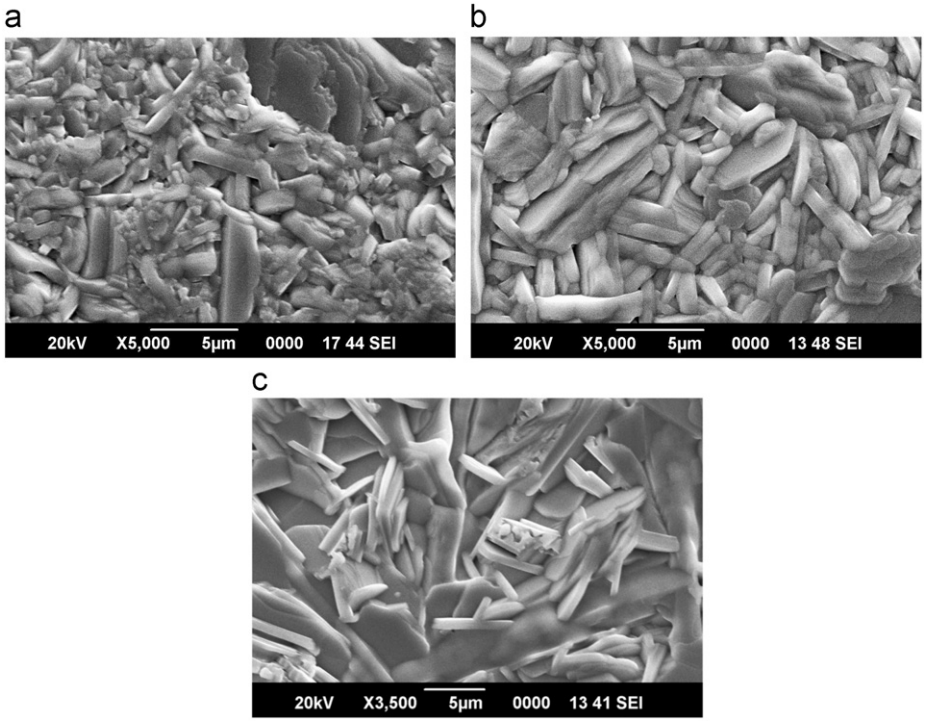

Fig. 5. (a) SEM image of $Ba_8MgNb_6O_{24}$ceramic, (b) SEM image of $Ba_8(Mg_{0.6}Zn_{0.4})Nb_6O_{24}$ ceramic and (c) SEM image of $Ba_8ZnNb_6O_{24}$ ceramic.

It is generally known that the variations of the microwave dielectric properties are closely related to the morphological changes of the dielectric ceramics [32]. In order to clarify the relationship between the microwave dielectric properties and the morphological change in the samples caused by the Zn substitution for Mg, the microstructures of the samples have been investigated by using SEM. Fig. 5(a)–(c), show the SEM images of $Ba_8MgNb_6O_{24}$, $Ba_8(Mg_{0.6}Zn_{0.4})Nb_6O_{24}$ and $Ba_8ZnNb_6O_{24}$, respectively. The surface of $Ba_8MgNb_6O_{24}$ exhibits minimal porosity and is comprised of ''bar'' and ''platelet-shaped rectangular'' grains. It was reported that the driving forces for densification and grain growth are comparable in magnitude, both being proportional to the reciprocal grain size in the sintering process [33]. The grains are in different size varying from few nanometers to micrometer scales. It is noted that there is a tendency of increasing the average grain size with the substitution of Zn for Mg. For $Ba_8(Mg_{0.6}Zn_{0.4})Nb_6O_{24}$, the grains are appeared as elongated bar and platelet-shaped in the microstructure and get more ordered. But in $Ba_8ZnNb_6O_{24}$, the needle shaped grains grows predominantly along the direction of platelet-shaped grains. Although the grain sizes of $Ba_8(Mg_{1-x}Zn_x)Nb_6O_{24}$ are increased with increasing composition x, the formation of porosities and secondary phases are not observed in the compositions ranging from 0 to 1. Thus, it is considered that the morphological changes in the samples cause the variation in the dielectric properties. As the grain size increased by the Zn-substitution, the $Q_u \times f$ values decreased. The EDS image of sintered $Ba_8ZnNb_6O_{24}$ ceramic given in Fig. 6 shows that all the constituent elements are present in the same stoichiometric concentrations which is in agreement with the reports by Thirumal and Davies where no loss of ZnO

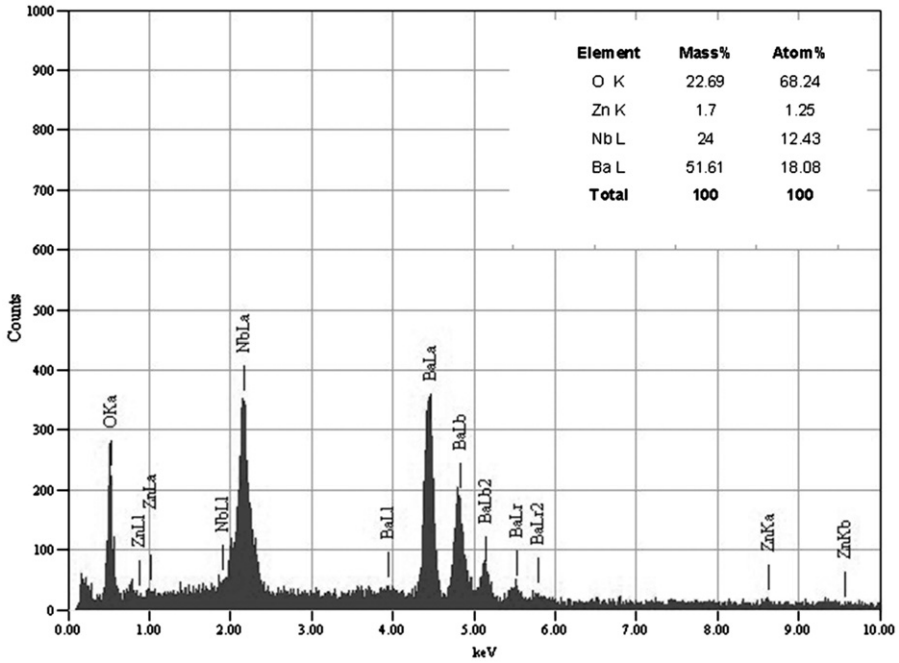

Fig. 6. EDS image of sintered $Ba_8MgNb_6O_{24}$ceramic.

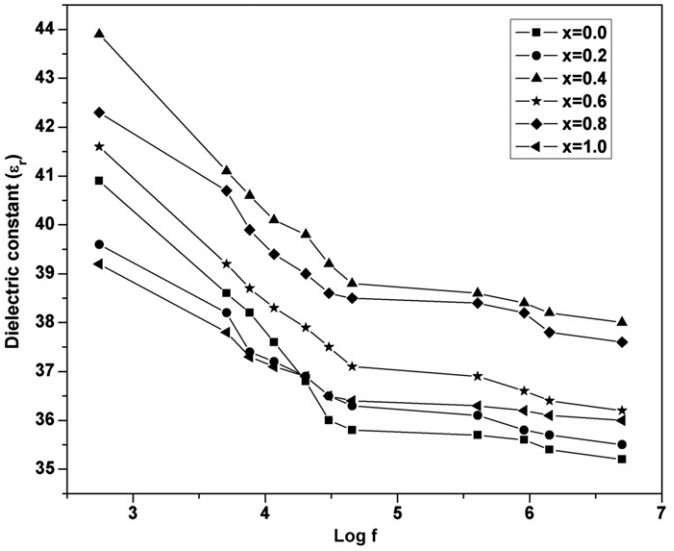

Fig. 7. Variation of dielectric constant (ε_r) with frequency.

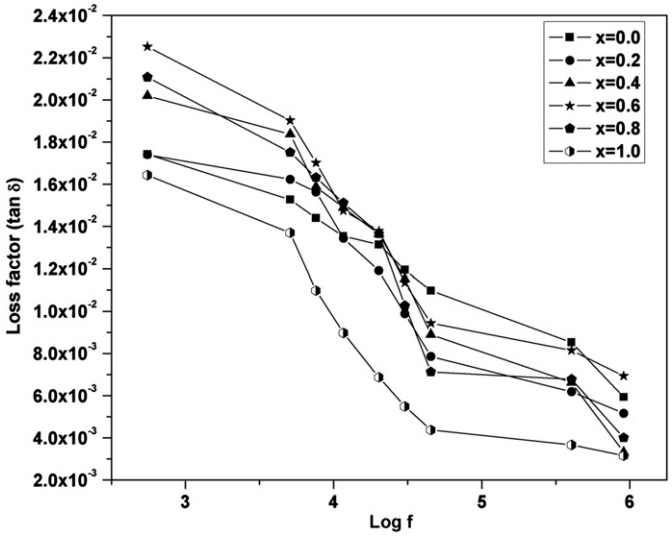

Fig. 8. Variation of loss factor (tan δ) with frequency.

and no formation of additional impurity phases were observed when $Ba_8ZnTa_6O_{24}$ was sintered at 1500 °C [17].

The dielectric properties of the sintered pellets are studied in the frequency range 50 Hz–5 MHz, at room temperature. The variation of dielectric constant (ε_r) with frequency ($\log f$) is shown in Fig. 7. The decrease in the dielectric constant with increasing frequency is attributed to Maxwell–Wagner interfacial polarization [34]. It is due to the fact that polarization does not occur instantaneously with the application of the electric field because of inertia. At low frequencies, all the polarizations contribute. When frequency increases, those with large relaxation time cease respond and results in the decrease in dielectric constant [35–37]. The values of dielectric constant (ε_r) are varying between the values 35.7 and 38.4, at 1 MHz, as similar to the trend that observed in microwave frequency region. The variation of loss factor (tan δ) with frequency is shown in Fig. 8 and it is observed that the loss factor is decreasing in the order of 10^{-2}–10^{-3} with the increase in frequency. The decrease of loss factor (tan δ) with the increase of frequency may be described on the basis of Koops phenomenological model [38]. In short, the dielectric constant and loss factor decrease with the increase in frequency for all the compositions.

4. Conclusions

$Ba_8(Mg_{1-x}Zn_x)Nb_6O_{24}$ ($x=0$, 0.2, 0.4, 0.6, 0.8 and 1) ceramics were prepared through conventional solid-state route. The materials were calcined at 1250 °C and sintered at 1375–1425 °C. The structure of the system was analyzed through XRD, Raman and FT-IR studies. No structural change was observed by the variation of x. The dielectric constant (ε_r), temperature coefficient of resonant frequency (τ_f) and the unloaded quality factor (Q_u) were measured in the microwave frequency region. The τ_f values of the samples reduced by varying the value of x from 0 to 1. The microstructure of the sintered pellets was analyzed using SEM and the variation of grain size caused the change in $Q_u \times f$ value. The dielectric responses to frequency were also studied in the range 50 Hz–5 MHz. The compositions have good microwave dielectric properties and hence are suitable for dielectric resonator applications.

Acknowledgment

The authors are thankful to Dr. M.T. Sebastian for his help in microwave measurements. Dr. Sam Solomon acknowledges University Grants Commission (UGC) for the post doctoral research award.

References

[1] S.J. Fiedziuszko, S. Holme, Dielectric resonators, IEEE Microwave Magazine 2 (9) (2001) 51–60.
[2] K. Wakino, T. Nishikawa, H. Tamura, T. Sudo, Dielectric resonator materials and their applications, Microwave Journal 30 (1987) 133–150.
[3] W. Wersing, Microwave ceramics for resonators and filters, Current Opinion in Solid State and Materials Science 1 (1996) 715–731.
[4] K. Wakino, T. Nishikava, Y. Ishikawa, H. Tamura, Dielectric resonator applications for mobile communications systems, British Ceramic Transactions and Journal 89 (1990) 39–43.
[5] I.M. Reaney, D. Iddles, Microwave dielectric ceramics for resonators and filters in mobile phone networks, Journal of the American Ceramic Society 89 (2006) 2063–2072.
[6] M.T. Sebastian, in: Dielectric Materials for Wireless Communication, first ed., Elsevier Publications, The Netherlands, 2008.
[7] K. Kakegawa, T. Wakabayashi, Y. Sasaki, Preparation of $Ba(Mg_{1/3}Ta_{2/3})O_3$ using oxine, Journal of the American Ceramic Society 69 (1986) C82–C83.
[8] D.A. Sagada, S. Nambu, Microscopic calculation of dielectric loss at microwave frequencies for complex perovskite $Ba(Zn_{1/3}Ta_{2/3})O_3$, Journal of the American Ceramic Society 75 (1992) 2573–2575.
[9] S. Kawashima, M. Nishida, I. Ueda, H. Ouchi, $Ba(Mg_{1/3}Ta_{2/3})O_3$ ceramics with low-dielectric loss at microwave frequencies, Journal of the American Ceramic Society 66 (1983) 421–426.
[10] S. Nomura, K. Toyama, K. Kaneta, $Ba(Mg_{1/3}Ta_{2/3})O_3$ ceramics with temperature stable high dielectric constant and low microwave loss, Japanese Journal of Applied Physics 21 (1982) L624–L626.
[11] S. Kawashima, M. Nishida, I. Ueda, H. Ouchi, S. Hayakawa, Dielectric properties of $Ba(Zn_{1/3}Nb_{2/3})O_3$–$Ba(Zn_{1/3}Ta_{2/3})O_3$ ceramics, in: Proceedings of the Ferroelectric Materials and Their Applications, vol. 1, 1977, pp. 293–296.
[12] S.-Y. Noh, M.J. Yoo, S. Nahm, C.H. Choi, H.-M. Park, H.-J. Lee, Effect of structural changes on the microwave dielectric properties of $Ba(Zn_{1/3}Nb_{2/3})O_3$ ceramics, Japanese Journal of Applied Physics 41 (2002) 2978–2981.
[13] S.B. Desu, H.M. O'Bryan, Microwave loss quality of $BaZn_{1/3}Ta_{2/3}O_3$ ceramics, Journal of the American Ceramic Society 68 (1985) 546–551.
[14] J.-I. Yang, S. Nahm, C.-H. Choi, H.-J. Lee, H.-M. Park, Microstructure and microwave dielectric properties of $Ba(Zn_{1/3}Ta_{2/3})O_3$ ceramics with ZrO_2 addition, Journal of the American Ceramic Society 85 (2002) 165–168.
[15] V. Tolmer, G. Desgardin, Low-temperature sintering and influence of the process on the dielectric properties of $Ba(Zn_{1/3}Ta_{2/3})O_3$, Journal of the American Ceramic Society 80 (1997) 1981–1991.
[16] S.J. Webb, J. Breeze, R.I. Scott, D.S. Cannell, D.M. Iddles, N.McN. Alford, Raman spectroscopic study of gallium-doped $Ba(Zn_{1/3}Ta_{2/3})O_3$, Journal of the American Ceramic Society 85 (2002) 1753–1756.
[17] M. Thirumal, P.K. Davies, $Ba_8ZnTa_6O_{24}$: a new high Q dielectric perovskite, Journal of the American Ceramic Society 88 (2005) 2126–2128.
[18] H. Hughes, F. Azough, R. Freer, D. Iddles, Development of surface phases in $Ba(Zn_{1/3}Nb_{2/3})O_3$–$Ba(Ga_{1/2}Ta_{1/2})O_3$ microwave dielectric ceramics, Journal of the European Ceramic Society 25 (2005) 2755–2758.
[19] P.K. Davies, A. Borisevich, M. Thirumal, Communicating with wireless perovskites: cation order and zinc volatilization, Journal of the European Ceramic Society 23 (2003) 2461–2466.
[20] M. Bieringer, S.M. Moussa, L.D. Noailles, A. Burrows, C.J. Kiely, M.J. Rosseinsky, R.M. Ibberson, Cation ordering, domain growth, and zinc loss in the microwave dielectric oxide $Ba_3ZnTa_2O_9$, Chemistry of Materials 15 (2003) 586–597.
[21] M. Barwick, F. Azough, R. Freer, Structure and dielectric properties of perovskite ceramics in the system $Ba(Ni_{1/3}Nb_{2/3})O_3$–$Ba(Zn_{1/3}Nb_{2/3})O_3$, Journal of the European Ceramic Society 26 (2006) 1767–1773.
[22] S. Kawaguchi, H. Ogawa, A. Kan, S. Ishihara, Microwave dielectric properties of $Ba_8Ta_6(Ni_{1-x}M_x)O_{24}$ (M=Zn and Mg) ceramics, Journal of the European Ceramic Society 26 (2006) 2045–2049.
[23] M.K. Suresh, J.K. Annamma John, P.R.S. Thomas, Sam Wariar, Solomon, Structural, spectroscopic and dielectric investigations on $Ba_8Zn(Nb_{6-x}Sb_x)O_{24}$ microwave ceramics, Materials Research Bulletin 45 (2010) 1389–1395.
[24] M.K. Suresh, Annamma John, J.K. Thomas, P.R.S. Wariar, Sam Solomon, Structural analysis and properties of thermally stable $Ba_8Mg(Nb_{6-x}Sb_x)O_{24}$ microwave ceramics, Journal of Alloys and Compounds 509 (2011) 2401–2406.
[25] B.W. Hakki, P.D. Coleman, A dielectric resonator method of measuring inductive capacities in the millimeter range, IRE Transactions on Microwave Theory and Techniques 8 (1960) 402–410.
[26] W.E. Courtney, Analysis and evaluation of a method of measuring the complex permittivity and permeability of microwave insulators, IRE Transactions on Microwave Theory and Techniques 18 (1970) 476–485.
[27] J. Krupka, K. Derzakowski, B. Riddle, J.B. Jarvis, A dielectric resonator for measurements of complex permittivity of low loss dielectric materials as function of temperature, Measurement Science and Technology 9 (1998) 1751–1756.
[28] S.M. Moussa, J.B. Claridge, M.J. Rosseinsky, S. Clarke, R.M. Ibberson, T. Price, D.M. Iddles, D.C. Sinclair, $Ba_8ZnTa_6O_{24}$: a high-Q microwave dielectric ceramic from a potentially diverse homologous series, Applied Physics Letters 82 (2003) 4537–4539.
[29] A.M. Abakumov, The crystal structure of $Ba_8Ta_6NiO_{24}$ cation ordering in hexagonal perovskites, Journal of Solid State Chemistry 125 (1996) 102–107.
[30] W.G. Fateley, F.R. Dollish, N.T. McDevitt, F.F. Bentley, Infrared and Raman Selection Rules for Molecular and Lattice Vibrations: The Correlation Method, Wiley-Interscience, John Wiley & Sons, New York, 1972.
[31] R. Ratheesh, M. Wöhlecke, B. Berge, Th. Wahlbrink, H. Haeuseler, E. Rühl, R. Blachnik, P. Balan, N. Santha, M.T. Sebastian, Raman study of the ordering in $Sr(B'_{0.5}Nb_{0.5})O_3$ compounds, Journal of Applied Physics 88 (2000) 2813–2818.

[32] S.J. Penn, N.McN. Alford, A. Templeton, X. Wang, M. Xu, M. Reece, Effect of porosity and grain size on the microwave dielectric properties of sintered alumina, Journal of the American Ceramic Society 80 (1997) 1885–1888.
[33] C.P. Cameron, R. Raj, Grain-growth transition during sintering of colloidally prepared alumina powder compacts, Journal of the American Ceramic Society 71 (1988) 1031–1035.
[34] J.C. Maxwell, A Treatise on Electricity and Magnetism, vol. 2, Oxford University Press, Oxford, U.K, 1954 Section 328.
[35] S.V. Pol, V.G. Pol, A. Gedanken, G.I. Spijksma, J. Grinblat, R.K. Selvan, V.G. Kessler, G.A. Seisenbaeva, S. Gohil, Synthesis of nanocrystalline zirconium titanate and its dielectric properties, Journal of Physical Chemistry C 111 (2007) 2484–2489.
[36] A.T. Raghavender, K.M. Jadhav, Dielectric properties of Al-substituted Co ferrite nanoparticles, Bulletin of Materials Science 32 (2009) 575–578.
[37] S. Chopra, S. Sharma, T.C. Goel, R.G. Mendiratta, Structural, dielectric and pyroelectric studies of $Pb_{1-x}Ca_xTiO_3$ thin films, Solid State Communications 127 (2003) 299–304.
[38] C.G. Koops, On the dispersion of resistivity and dielectric constant of some semiconductors at audiofrequencies, Physical Review 83 (1951) 121–124.